 doi:10.20944/preprints202110.0138.v1

Article

Green synthesis of Hexagonal Hematite (α-Fe_2O_3) flakes using Pluronic F127-Gelatin template for adsorption and photodegradation of ibuprofen

Maria Ulfa [1,*], Didik Prasetyoko [2], Hasliza Bahruji [3] and Reva Edra Nugraha [4]

[1] Chemistry Education Study Program, Faculty of Teacher Training and Education, Sebelas Maret University, Jl. Ir. Sutami 36A, Surakarta 57126, Central Java Indonesia
[2] Department of Chemistry, Faculty of Science, Institut Teknologi Sepuluh Nopember, Keputih, Sukolilo, Surabaya 60111, East Java, Indonesia
[3] Centre of Advanced Material and Energy Sciences, University Brunei Darussalam, Jalan Tungku Link, BE1410 Darussalam, Brunei
[4] Department of Chemical Engineering, Faculty of Engineering, Universitas Pembangunan Nasional "Veteran" Jawa Timur, Surabaya, East Java, 60294, Indonesia
* Correspondence: ulfa.maria2015@gmail.com

Abstract: Hematite (α-Fe_2O_3) with uniform hexagonal flakes morphology has been successfully synthesized using a combination of gelatin as natural template with F127 via hydrothermal method. The resulting hematite was investigated as adsorbent and photocatalyst for removal of ibuprofen as pharmaceutical waste. Hexagonal flake-like hematite was obtained following calcination at 500 °C with the average size was measured at 1-3 μm. Increasing the calcination temperature to 700 °C transformed the uniform hexagonal structure into cubic shape morphology. Hematite also showed high thermal stability with increasing the calcination temperatures, however, the surface area was reduced from 47 m^2/g to 9 m^2/g. FTIR analysis further confirmed the formation Fe-O-Fe bonds, and the main constituent elements of Fe and O were observed in EDX analysis for all samples. Fe_2O_3-G samples have an average adsorption capacity of 55-25.5 mg/g at 12-22% of removal efficiency when used as adsorbent for ibuprofen. The adsorption capacity was reduced with increasing the calcination temperatures due to the reduction of available surface area of the hexagonal flakes when transformed into cube. Photocatalytic degradation of ibuprofen using hematite flakes achieved 50% of removal efficiency meanwhile combination of adsorption and photocatalytic degradation further removed 80% of ibuprofen in water/hexane mixtures.

Keywords: α- Fe_2O_3, hematite, gelatin, f-127, hexagonal-flake, adsorption, ibuprofen

1. Introduction

Hematite has been widely investigated as adsorbent for removal of dye, pharmaceutical compound, heavy metal and industrial waste (Chibowski, 2014; Elazhari & Abouarnadase, 2020; Engwayu & Pawlik, 2020; Quast, 2018). Hematite is also referred as α-Fe_2O_3, which is one of the most thermodynamically stable types of iron oxide because of the strong interaction between the electrons (Mamindy-pajany et al., 2011). Hematite structure resembles corundum, in which the Fe^{3+} cations are connected to the octahedral oxygen via the covalent bonds in a hexagonal closed packing crystal system (Quast, 2018). Hematite was reported to have high adsorption performance and stability, and is easy and cheap to synthesize (Al-Hakkani et al., 2021; Chibowski, 2014; Grimm et al., 1997; Watanabe et al., 1994). The surface area of hematite was reported between 10-90 m^2/g, thus showed ability as adsorbent in the removal of cephalecin, acetylsalicylic acid, congo red, and heavy metals (Elazhari & Abouarnadase, 2020; Engwayu & Pawlik, 2020). The hydrophilicity of hematite is reasonably high which is beneficial for the adsorption of many organic molecules in water (Noerpel & Lenhart, 2015). In addition, the presence of

Preprints (www.preprints.org) | NOT PEER-REVIEWED | Posted: 8 October 2021 doi:10.20944/preprints202110.0138.v1

Fe^{3+} ion and the surface OH group formed chemical and physical interaction with organic molecules (Elazhari & Abouarnadase, 2020; Yang et al., 2015). Hematite was reported to prevent flotation when used as adsorbent for oleate (Quast, 2018). Antistereoidal agent waste such as ibuprofen polluted water and land when discharged from the hospital drainage untreated (Guedidi et al., 2017). Removal of ibuprofen was carried out via high temperature decomposition or with the use of solvent (Guedidi et al., 2017; Mondal et al., 2016; Varghese & Ghoroi, 2017). The used of solvent to remove ibuprofen is less environmentally friendly, meanwhile the high temperature decomposition method requires a large amount of energy.

Hematite is naturally available in abundance, non-toxic to environment, and its chemical activity was greatly influenced by its multiple oxidation states. Hematite can be synthesized using sol gel, arc-discharge, micro-emulsion, thermal decomposition, hydro-thermal synthesis, ball milling, sol gel, hydrometallurgy, electrolysis and co-precipitation (Al-Hakkani et al., 2021). Another method that received increasing attention is preparation of iron oxide using a green templating method. The use of synthetic structure directing agents such as P-123, F-127, cetyl trimethylammonium bromide and cetyl trimethylammonium chloride (Hu et al., 2011; Liu et al., 2013; Nagamine et al., 2001; Ulfa et al., 2011; al., 2020) can be minimized by replacing the template with biodegradable natural reagents. Green synthesis is also beneficial to minimize the production of residual waste from utilization of hazardous chemical reagents (Al-Hakkani et al., 2021). Green synthesis using plant extract from green tea, kurkuma and lantana fir leaves produced hematite with rod, hexagonal, cone cube and flake structures (Al-Hakkani et al., 2021; Upadhyay et al., 2020). However, a high concentration of plant extract was required for rearrangement of the molecules to form uniform structure. The plant extract was unable to direct the formation of pore and prone to reduction lead to deactivation of molecular rearrangement process. Therefore, stabilization of plant extract during the synthesis is required either via pH variation, temperature or time regulation and some reactions required nitrogen gas to increase the stability. In addition, plant extract also formed a residual by-product on the synthesized material that can interfere with the characterization and the application processes (Khani et al., 2017; Nasirian et al., 2017; Seo et al., 2018; Vargas et al., 2020). The use of plant extract can be replaced using extract from animal such as gelatin. Gelatin derived from the hydrolysis of animal skin and bone waste has a fairly stable amine group that can form a strong affinity with precursor as pore director in the molecular rearrangement process (Bele et al., 2002; Coradin et al., 2004).

Apart from its performance as adsorbent, hematite has 2.1-2.3 eV band gap which is suitable as photocatalyst for photodegradation of pollutants (Cao et al., 2020; Sugrañez et al., 2015). The conduction band of hematite is composed of empty orbitals in the *d* band of Fe^{3+} and the valence band from the 3d crystal plane that was filled with Fe^{3+} from the formation of 2p non-bonding orbitals (Ogi et al., 2016). The semiconductor property causes hematite to be widely used as photocatalysts, pigments, gas sensors (Barthe et al., 2008; Grimm et al., 1997; Noerpel & Lenhart, 2015). We have previously reported that the combination of gelatin with block copolymer F127 produced carbon materials with variation of shapes such as carbon foam worm-holes and mesoporous carbon microspheres with high surface area up to 220 m^2/ g (Ulfa et al., 2016, 2020). Since green synthesis of hematite requires a high stability of template that promises a high regeneration power, this research aimed to synthesis hematite using a combination of gelatin and F127 as a structure directing agents. The structural properties of hematite was investigated by variation of calcination temperatures between 500-700 °C. We observed transformation of flake-like morphology to cubic structure with increasing the calcination temperatures. The α-Fe_2O_3 flakes were utilized as adsorbent and photocatalyst for removal of ibuprofen as pharmaceutical waste.

Preprints (www.preprints.org) | NOT PEER-REVIEWED | Posted: 8 October 2021 doi:10.20944/preprints202110.0138.v1

2. Experiment

2.1. Preparation Of Hexagonal Flake-Like Of Hematite (A-Fe_2O_3) by Gelatin Template

Ferric chloride ($FeCl_3$, MW 162.20, reagent grade 97%), Pluronic F127, HCl, gelatin and ibuprofen (2-[4-(2-methylpropyl) phenyl] propanoic acid) were obtained from Sigma Aldrich and used without prior pretreatment. For the synthesis of hematite flake, Pluronic F127 powder was added into HCl solution and stirred in room temperature for 24 h. The gelatin powder was then added into the mixture followed by ferric chloride. The mixture was stirred until homogeneous solution was formed. The weight ratio of the synthesis materials was used as follows: 1 Pluronic F127: 0.05 gelatin: 5 Ferric chloride: 0.015 HCl. The resulting homogeneous mixture was then poured into autoclave with Teflon liner and heated at 100 °C for 24 h. The solid was filtered and calcined at 500 °C for 5 h. Finally, the black powder was washed, filtered and dried overnight at 100 °C. The temperature of calcination was increased to 600 °C and 700 °C to obtain hematite sample which labeled is Fe_2O_3-G-xC which x is the calcination temperature.

2.2. Characterization

The crystalline phase of hematite was investigated using X-ray diffraction, XRD. XRD pattern was obtained by Philips X'pert XRD instrument with Cu Ka radiation with a step size of 0.04° and counting time of 10 s. The data were recorded in the 2θ between 5-80°. The crystallinity of iron oxide was calculated based on the ratio of the area of the crystalline peaks to the total area under all peaks as shown by equation 1 (Yatsenko & Medvedeva, 2019).

$$\text{Crystallinity} = \frac{\text{Total area of crystalline peaks}}{\text{Total area of all peaks}} \qquad \text{Eq 1.}$$

The morphology of the samples and elemental composition were analysed using Scanning Electron Microscopy (SEM) ZEIS EVO MA 10 and coated by Pd/Au and energy dispersive X-ray spectroscopy (EDS). Surface area of the sample was measured using nitrogen as adsorbate at P/P0–0.99 by the BET method. The BJH and SF method were used to determine the size of mesopore and micropore, respectively. The thermal gravimetric analysis was conducted at a heating rate of 10 °C min^{-1} from room temperature to 1200 °C under argon. The functional group of the materials were characterized through Fourier transform Infrared spectroscopy (Nicolet 6700 FTIR instrument).

2.3. Ibuprofen Adsorption

To investigate the adsorption profiles of hematite, ibuprofen solution was prepared in water-hexane (1:1 v/v) at 100 mgL^{-1} of initial concentration. The concentration of ibuprofen was monitored using UV–Vis spectroscopy at 272 nm wavelength. The calibration was carried using ibuprofen standard solutions with concentration of 5– 100 mg L^{-1}. 50 mg of the resulting hematite were added into 50 mL of ibuprofen solution and stirred at room temperature for 30 min. 3 mL of ibuprofen solution were sampled every 5 min intervals and separated using membrane filter followed by UV–Vis measurement. The analysis was carried out until the adsorption reached equilibrium. The adsorption was repeated up to 60 min to monitor the stability of the ibuprofen adsorption on hematite. UV–Vis analysis was performed using U-2000 Hitachi Japan. The calculation of the adsorption capacity and the adsorption kinetics were based the previous research (Ulfa et al., 2020) as shown in the following equation:

$$q_e = (Co - Ce)(\frac{v}{w}) \qquad \text{(Eq. 2)}$$

Where q_e (mg / g) is the adsorption capacity in equilibrium, while Co, Ce, v and w are the initial concentration (mg / L), concentration of ibuprofen in equilibrium (mg / L), volume of ibuprofen (L), respectively, and adsorbent weight (mg) Co and Ce. Meanwhile, the adsorption kinetics follows the pseudo first order by Lagergren equation:

Preprints (www.preprints.org) | NOT PEER-REVIEWED | Posted: 8 October 2021 doi:10.20944/preprints202110.0138.v1

$$\ln(q_e - q_t) = \ln q_e - k_1 t \qquad \text{(Eq. 3)}$$

And the pseudo second order equation by Ho McKay follows:

$$\frac{t}{q_t} = \frac{1}{k_2(q_e)^2} - \frac{1}{q_e} t \qquad \text{(Eq. 4)}$$

The linearity value of R2 plotted t vs $\ln(q_e - q_t)$ dan t vs t/qt will be used to determine the appropriate kinetics for the adsorption of ibuprofen using iron oxide in this study.

2.4 Photocatalytic degradation of ibuprofen

Photocatalytic activity of iron oxide in the degradation of ibuprofen was determined using UV light at wavelength of 265 nm. Ultraviolet irradiation was monitored using a spectroradiometer (Lumen spectroradiometer-Stellarnet-20 mA). Photocatalytic degradation was carried out by adding 5 ml of ibuprofen solution (5 mg/L) and 2 mg of hematite into a quartz tube and irradiated with UV light at different time intervals such as 20, 30, 40, 50, 70, 90, 120 min under continuous stirring. Three separate experiments were carried out, in dark, under immediate light irradiation and 20 min dark adsorption prior to UV irradiation. The percentage of ibuprofen degradation was calculated as follows:

$$\% \text{ Removal} = ((Co - C_t)/Co)) * 100$$

where Co and C_t represent ibuprofen concentration in the solution before and after the UV irradiation respectively.

3. Results and Discussion

3.1 XRD analysis

Figure 1 shows the X-ray diffractogram of hematite synthesized using F127-gelatin as structure directing agent (Fe_2O_3-G) after calcination at 500 °C, 600 °C, and 700 °C. The main peaks for α- Fe_2O_3 (JCPDS-850897) were observed at 24.08°; 33.10°; 35.56°, 40.96°; 49.52°; 54.24°; 57.82° with the respective miller field of (012); (104); (311); (113); (024); (116); and (018). The XRD of the synthesized hematite is also in accordance with the literatures (Watanabe et al., 1994; Zhang et al., 2016)). When the calcination was increased from 500 °C to 700 °C, there were no significant differences on the position of hematite peaks suggesting the stability of hematite. However, the peak at 33.10° (104) and 40.96° (113) which were exclusive to α- Fe_2O_3 showed a higher intensity as the calcination temperatures increased to 700 °C. The result suggests the conversion of γ-Fe_2O_3 to α-Fe_2O_3. At 500 °C, the XRD data also showed a broad peak at 20-30° due to the formation amorphous structure in hematite (Zhang et al., 2016). The amorphous structure was suggested as the result of incomplete decomposition of F127 and gelatin, leaving residual amorphous carbon. However, following calcination at 600 °C and 700 °C, the broad amorphous peaks were slightly reduced due to the elimination of residual amorphous carbon. The result was further supported by EDX data (table 1) which showed the samples contained 3.18% and 0.75% of carbon after calcination at 500 °C and 600 °C, respectively. However, at 700 °C carbon was completely removed from the sample resulting in the formation of high purity hematite. The crystallinity of iron oxides was calculated based on the ratio of the area of the crystalline peaks over the total area including the broad amorphous peak. Increasing the calcination temperatures from 500 °C to 700 °C significantly enhanced the crystallinity from 48.31% to 63.19% (Table 1).

Preprints (www.preprints.org) | NOT PEER-REVIEWED | Posted: 8 October 2021 doi:10.20944/preprints202110.0138.v1

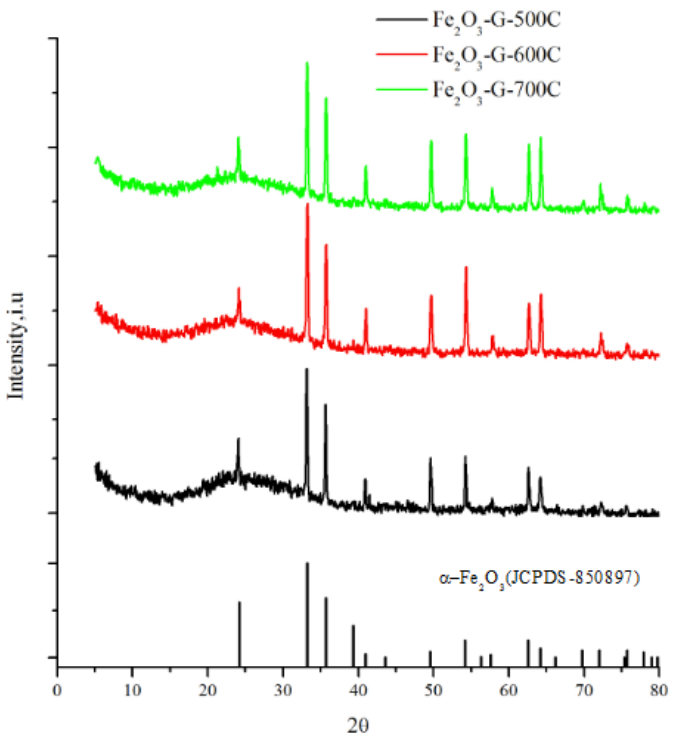

Figure 1. XRD of hematite synthesized with F127-gelatin after calcination at a. 500 °C, b. 600 °C and c 700 °C for 5 h.

Table 1. Crystallite size and elemental composition of hematite at different calcination temperatures.

Sample	[a]Crystallite size (µm)	[b]Crystallinity (%)	[c]Elemental composition%			
			C	O	Fe	Others
Fe_2O_3-G-500C	1.0-3.0	48.31	3.18	21.82	74.32	0.68
Fe_2O_3-G-600C	4.0-5.0	57.88	0.75	17.17	80.07	2.01
Fe_2O_3-G-700C	1.0-2.0	63.19	0	17.15	82.85	0

[a]determine from SEM analysis
[b]determine from XRD analysis
[c]determine from SEM-EDX analysis

3.2 SEM analysis

Figure 2 showed the SEM analysis of hematite calcined at 500 °C, 600 °C and 700 °C together with the particle size distribution histograms. As evidence from EDX analysis, calcination at high temperatures were important for removal of carbon residues originated from decomposition of the template. SEM analysis indicated significant structural changes following calcination at high temperatures. At 500 °C, hematite showed the formation of uniform flake-like hexagonal shape. The particle size histogram exhibited a narrow distribution with the average size was determined between 1-3 µm. When the calcination temperature was increased to 600 °C, the uniformity of the flake-like hexagonal structure was deteriorated, with apparent structural disintegration to form smaller aggregates. Nevertheless, the flake-like hexagonal structures were still visible and the size was increased to 4-5 µm. The presence of F127 and gelatin as template was responsible to enhance the structural stability of iron oxide in order to maintain the flake-like hexagonal structure after calcination at 600 °C. Following calcination at 700 °C, transformation from flake-like hexagonal structure to cube was observed, and the size reduced to 1-2 µm. In the synthesis of iron oxide, calcination at 500 °C is important for the formation of bonds between the iron oxide grains (Li et al., 2021; Shah & Rather, 2020). However, calcination

Preprints (www.preprints.org) | NOT PEER-REVIEWED | Posted: 8 October 2021 doi:10.20944/preprints202110.0138.v1

at 700 °C was important to remove carbon impurities, although the morphology was transformed from hexagonal flake-like structure into cubic structure.

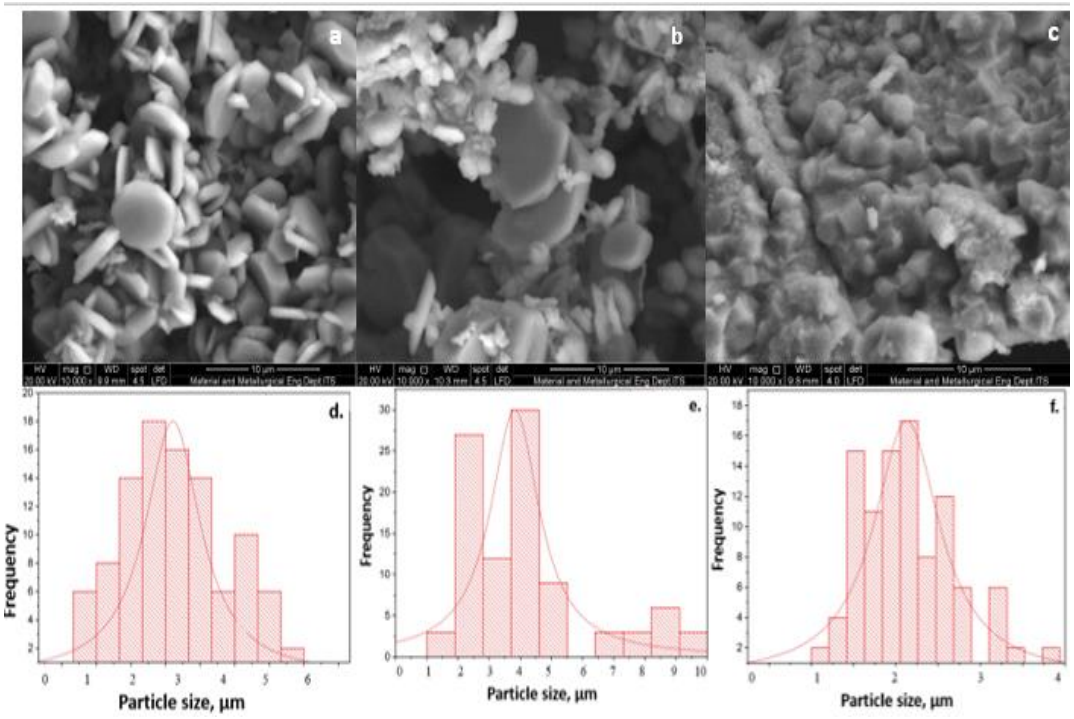

Figure 2. SEM of iron oxide synthesized after calcination at a. 500 °C, b. 600 °C and c 700 °C for 5h

Characterization results obtained from XRD and SEM analysis provided insight into the stability of α-Fe_2O_3 morphology. Although α-Fe_2O_3 was calcined at 500 °C in order to remove the template during the synthesis, the flake-like structures were retained and stable up to 600 °C. The ability to direct the morphology strongly relied on the presence of F127 and gelatin to form a stable micellar structure (Ulfa et al 2020). The OH functional groups in the copolymer block F127 and NH on the gelatin have a strong affinity for interacting with the iron precursor, so that these two molecules were able to direct the structure of the material (Ulfa et al., 2020). Gelatin consists of carboxyl, amino and hydroxyl groups acted as sites to form coordination with metal ionic species (Coradin et al., 2004). Fe^{2+}-gelatin complex formation stabilized iron from dissolution.(Haruna et al., 2018). However, due to the stability of block copolymer F127 and gelatin interaction with the elemental iron, decomposition at 700 °C is crucial to fully remove the residual carbon. The presence of carbon residue was still observed after calcination at 500-600 °C suggesting the strong interaction between iron and gelatin to maintain flake structures. However, as the temperature increased to 700 °C, the transformation of flake-like structure to cubic morphology occurred together with the removal of carbon impurities. The results further implied the role of gelatin to improve the stability of α-Fe_2O_3.

Preprints (www.preprints.org) | NOT PEER-REVIEWED | Posted: 8 October 2021 doi:10.20944/preprints202110.0138.v1

3.3 N_2 adsorption analysis

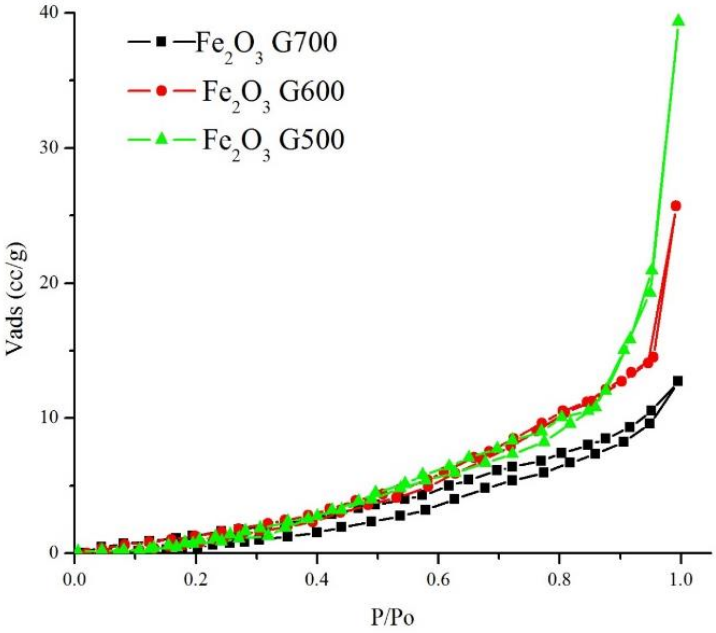

Figure 3. Nitrogen adsorption-desorption analysis of iron oxide synthesized using F127-gelatin after calcination at a. 500 °C, 600 °C and 700 °C for 5 h.

Figure 3 showed the nitrogen adsorption isotherm of iron oxide following calcination in air at 500 ℃, 600 ℃ and 700 ℃ for 5 h. The N_2 isotherm showed a typical type-III isotherm with the H1 hysteresis loop without capillary condensation which is the characteristic of a non-porous material. The specific surface area of α- Fe_2O_3 oxides after calcination of 500 ℃ was 49 m^2/g. The surface area was significantly reduced to 16 m^2/g following calcination at 600 °C and further reduced to 7 m^2/g when calcined at 700 °C. The pore volume analyzed using BJH method indicated the reduction from 0.161 cc/g to 0.030 cc/g when α- Fe_2O_3 was calcined from 500 ℃ to 700 ℃. The surface area and the pore volume summarized in Table 2 were significantly influenced by the calcination temperatures, due to the transformation of crystallite structure of iron oxide.

Although the synthesized hematite showed the typical non-porous isotherm, the presence of hysteresis loop at high pressures indicated the formation of macroporous originated from the interparticle interaction. The plot of pore size distribution in Fig 4 showed the average pore diameter was increased at high calcination temperatures from 37 Å when calcined at 500 ℃ to 83 Å when calcined 700 ℃. The increase of pore size presumably due to the decomposition of carbon from the F127 and gelatin copolymer composite that was previously occupied the vacant sites between the iron oxide particles. The decomposition of carbon at high temperatures also increased the possibility for the formation of pores as new cavities due to the loss of macromolecules carbon during its decomposition. From the SEM analysis, the macropores or mesopores region cannot be determined because SEM produced a three-dimensional image of the iron oxide aggregates. Therefore, the porosity was determined by using N_2 adsorption-desorption isotherm plot as well as the pore size distribution plot.

Table 2. Textural properties of Fe_2O_3-G obtained from N_2 adsorption-desorption analysis.

SAMPLE	S_{BET}	V tot	R(A)
Fe_2O_3-G-500C	49	0.1661	37.120
Fe_2O_3-G-600C	16	0.0275	43.32
Fe_2O_3-G-700C	7	0.0301	83.350

Preprints (www.preprints.org) | NOT PEER-REVIEWED | Posted: 8 October 2021 doi:10.20944/preprints202110.0138.v1

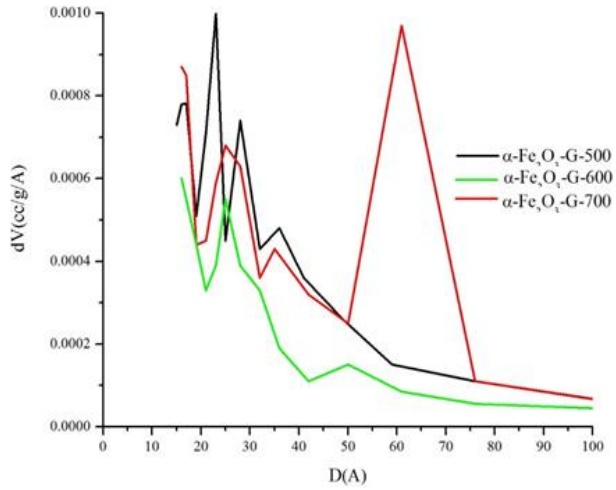

Figure 4. Pore size distribution of iron oxide synthesized with F127-gelatin after calcination at a. 500 °C, b. 600 °C and c 700 °C for 5 h.

TGA analysis

The TGA profiles of hematite after calcination of 500 °C, 600 °C and 700 °C showed the decomposition pattern upon annealing at high temperatures (Fig 5). The decomposition data calculated from TGA analysis were summarized in Table 3. The TGA showed initial decomposition at temperature between 50 to 90 °C with a significant decrease in weight at ~ 2-12%. The weight loss was due to the evacuation of physisorbed water or volatile compounds. The second decomposition stage showed a continuous increased of weight when the temperature was increased from 150 to 1000 °C. Annealing at high temperatures was suggested to increase the density of iron oxide due to the rearrangement of Fe-O-Fe bond following evacuation of carbonaceous contaminants. In general, the sample that was calcined at 700 °C has the highest thermal stability which was characterized by the low reduction in weight loss throughout the measurement.

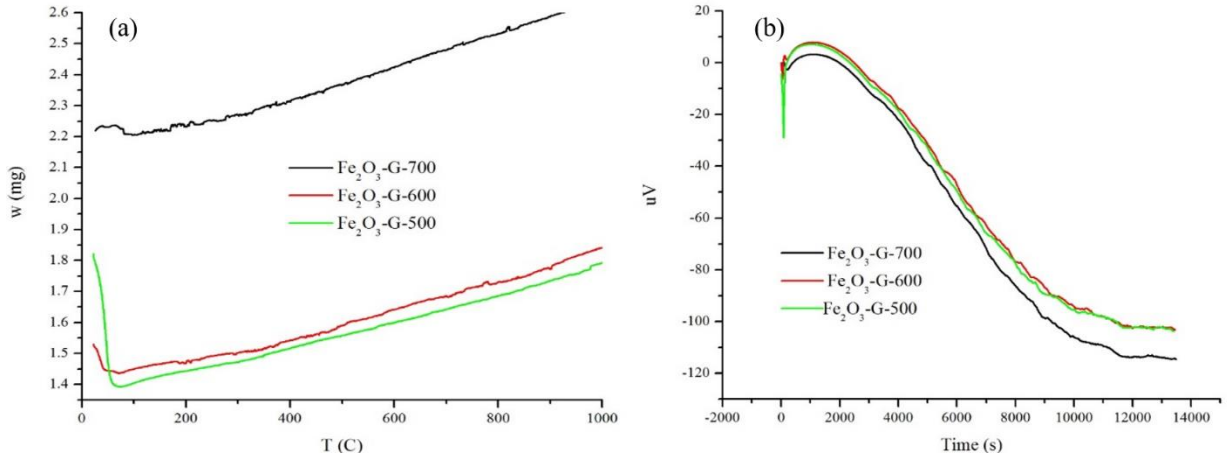

Figure 5. TGA (a) and DTA (b) of the synthesized iron oxide after calcination at 500 °C, 600 °C and 700 °C for 5 h

Table 3. Weight loss profile of Fe_2O_3-G obtained from TGA analysis.

Sampel	Weight loss (%)	Weight increases (%)
	0-150 °C	**150-1000** °C
Fe_2O_3-G 500	12.52	-25.2
Fe_2O_3-G 600	5.80	-13
Fe_2O_3-G 700	2.25	-10

Preprints (www.preprints.org) | NOT PEER-REVIEWED | Posted: 8 October 2021 doi:10.20944/preprints202110.0138.v1

3.5 Ibuprofen removal via adsorption

Figure 6 showed the adsorption of ibuprofen on hematite in 60 min of contact times. The amount of adsorbed ibuprofen was analysed on the resulting iron oxides after calcination of 500 °C, 600 °C and 700 °C. The results showed rapid adsorption within the first 30 minutes, followed by gradual adsorption before reaching equilibrium at 50 minutes. This was due to the decrease of surface area upon adsorption with ibuprofen, thereby reducing the availability of active binding sites at the saturation point as the adsorption reaching the equilibrium. The maximum adsorption capacity was determined on iron oxide calcined at 500 °C with the adsorption capacity was measured at 55.51 mg/g. When iron oxide calcined at 600 °C was used, the adsorption reduced to 42.12 mg/g and further reduction to 25 mg/g on iron oxide calcined at 700 °C. The removal efficiency was decreased from 22.2 % to 11.1 % with increasing the calcination temperatures up to 700 °C. The decrease in surface area of iron oxide when calcined at high temperature reduced the number available sites for ibuprofen adsorption. The adsorption of ibuprofen on α-Fe_2O_3-G500 occurs on the expose active site consisted of dangling Fe bond which form interaction with the OH group in ibuprofen (Yin et al., 2018).

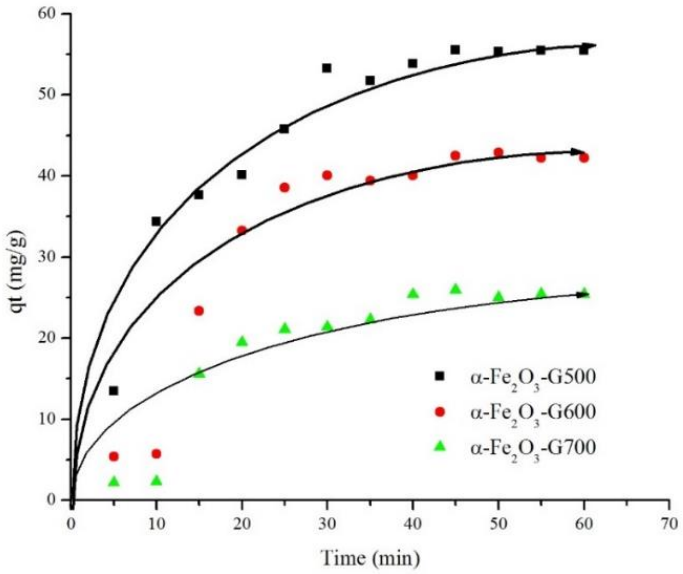

Figure 6. The effect of contact time on ibuprofen adsorption (50mg/L) while using hematite after calcination at 500 °C, 600 °C and 700 °C.

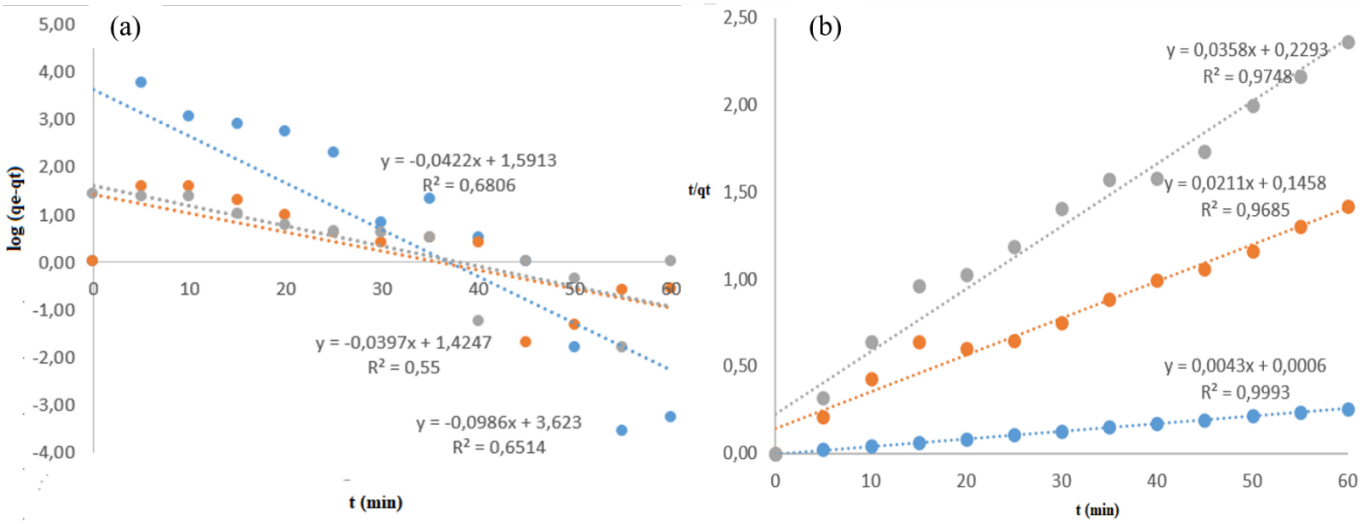

Figure 7. (a). Pseudo first order plot and (b). Pseudo second order plot of the kinetic of adsorption. — Iron oxide calcined at 500 °C, — calcined at 600 °C, and — calcined at 700 °C

Table 4 summarized the kinetic analysis data using the pseudo first order and the pseudo second order equations. The plot between ln(qe-qt) versus t for the pseudo-first-

Preprints (www.preprints.org) | NOT PEER-REVIEWED | Posted: 8 October 2021 doi:10.20944/preprints202110.0138.v1

order model (Fig 7a) and t/qt versus t plot for the pseudo-second-order model (Fig 7b) were carried out to obtain the regression coefficient value related to linearity (R2). The pseudo first order plot showed the R2 values for all the sample were within 0.5-0.7. Whereas for the pseudo second order plot, the R2 value of each calcined samples were closed to 1 thus indicating the adsorption of ibuprofen on Fe_2O_3-G followed the pseudo-second kinetic model.

Table 4. Kinetics of ibuprofen adsorption using iron oxide sample

sample	Co (ppm)			Pseudo First order			Pseudo Second order		
		qe exp (mg/g)	Removal efficiency, %	qe cal (mg/g)	k1(min^{-1})	R2	qe cal (mg/g)	k2($g.mg^{-1}.min^{-1}$)	R2
Fe_2O_3-G-500	100	55.51	22.2	419.7	0.0986	0.6514	55.55	0.083	0.999
Fe_2O_3-G-600	100	42.12	16.7	390.7	0.0901	0.524	41.66	0.078	0.963
Fe_2O_3-G-700	100	25.61	11.1	337.7	0.0926	0.5514	25.28	0.058	0.976

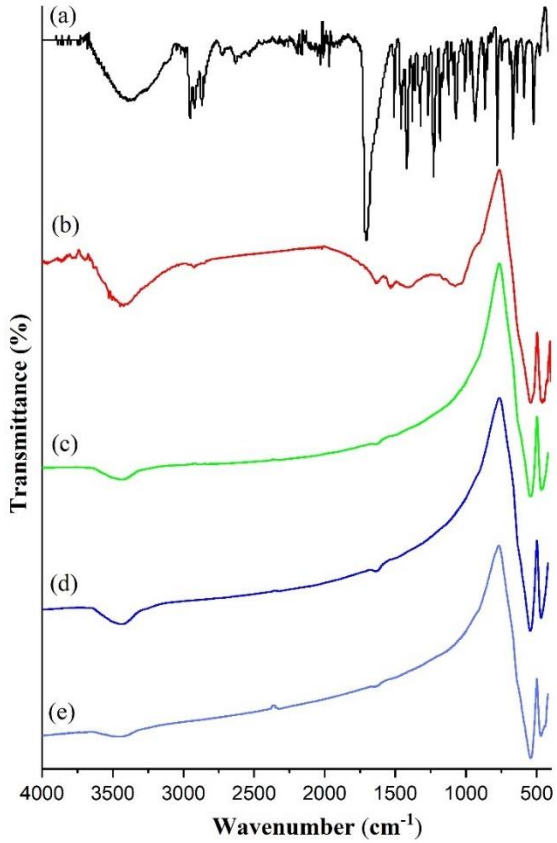

Figure 8. FTIR of (a). ibuprofen, b). Fe_2O_3-G500 after ibuprofen adsorption and Fe_2O_3-G iron oxide synthesized with F127-gelatin after calcination at (**c**). 500 °C, (**d**). 600 °C (e) 700 °C for 5h (before ibuprofen adsorption)

FTIR analysis was carried out to determine the adsorption of ibuprofen on hematite. Figure 8 showed a broad band between 3000 and 3500 cm^{-1} and small band at 1624 cm^{-1} which indicated the stretching vibration of hydroxyl group or physisorbed water. The strong adsorption on hematite samples at 431 cm^{-1} and 577 cm^{-1} corresponded to the Fe-O bond vibrations (Watanabe et al., 1994). There was no visible change in the intensity of the adsorption bands for iron oxide samples after calcination up to 700 °C. Figure 8 also showed that ibuprofen has an intense and well-defined infrared band at 1700-2100 cm^{-1} which is associated with the stretching of the C=O carbonyl group of ibuprofen (Yetiz et al., 2011). Following adsorption with ibuprofen on Fe_2O_3-G500, new the adsorption bands

Preprints (www.preprints.org) | NOT PEER-REVIEWED | Posted: 8 October 2021 doi:10.20944/preprints202110.0138.v1

appeared at 2929 cm^{-1} assigned to C-H vibration of ibuprofen, 1634 cm^{-1} due to C=O vibration, 1527 cm^{-1} corresponded to C=C vibration and 1064 cm^{-1} originated from C-O bond in the alcohol functional group in ibuprofen (Campos et al., 2020). The shifting of C=O absorption band at 1709 cm^{-1} in ibuprofen to 1634 cm^{-1} on adsorbed Fe_2O_3 implied a weaken C=O bond due to interaction with iron oxide.

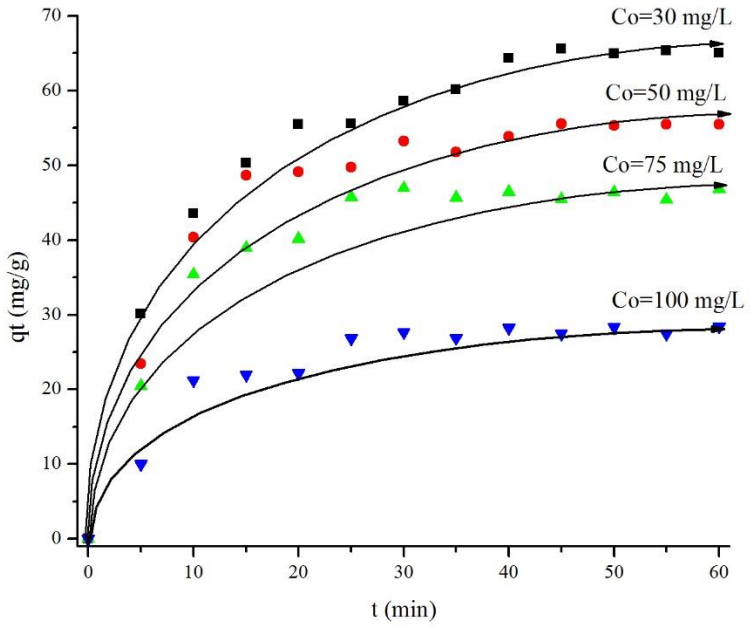

Figure 9. Effect of initial concentration of ibuprofen at a.100 mg/L, b. 75 mg/L, c. 50 mg/L during adsorption using Fe_2O_3-G-500

The effect of ibuprofen concentration on adsorption capacity was investigated using Fe_2O_3-G-500 at 30 mg/L, 50 mg/L 75 mg/L and 100 mg/L. Fig 9 showed that the adsorption capacity decreased gradually from 64 mg/g to 28 mg/g with increasing concentration of ibuprofen. This phenomenon is probably due to the presence of concentration gradient that causes a change in the driving force of ibuprofen into the adsorbent (Das et a., 2015). Furthermore, the surface area of iron oxide is relatively smaller than that of most adsorbent, thus unable to adsorb a high cocentration ibuprofen resulting in the decrease of adsorption capacity (Satapathy et al., 2013). The decrease of adsorption sites saturated with ibuprofen molecules is predicted to have a strong influence in decreasing the adsorption capacity by two times, as observed in 50mg/L and 100mg/L of ibuprofen concentrations (Banerjee et al, 2016).

Preprints (www.preprints.org) | NOT PEER-REVIEWED | Posted: 8 October 2021 doi:10.20944/preprints202110.0138.v1

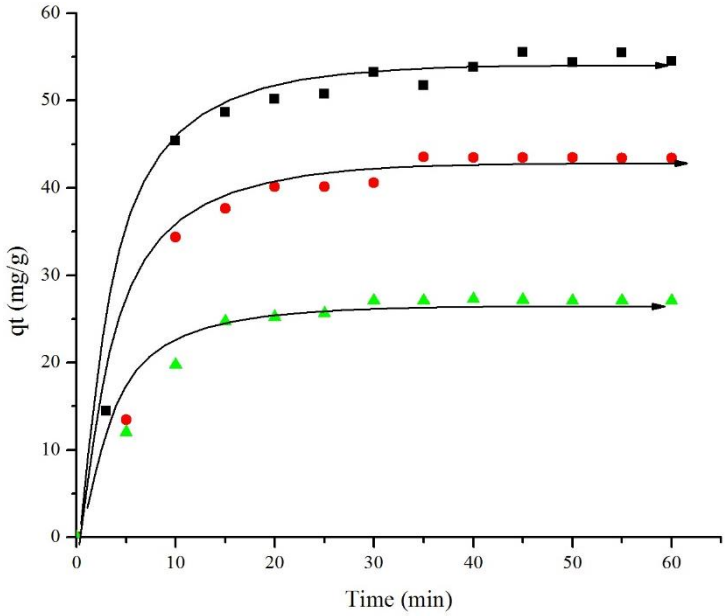

Figure 10. Effect of temperature at room temperature (black square), 35 °C (red circle) and 45 °C (green triangle) during ibuprofen adsorption using Fe_2O_3-G-500.with initial concentration 50 mg/L

Figure 10 illustrates the effect of temperature on the adsorption capacity of ibuprofen while using Fe_2O_3-G-500 as adsorbent. The adsorbed capacity was reduced from 55 mg/g at room temperature to 22 mg/g at 45 °C within 60 minutes. The decrease in adsorption capacity at high temperature implied the reduction of physical interaction between ibuprofen and the iron oxide active site. High temperature also increased the diffusion rate of ibuprofen from the surface of adsorbent and improved repulsion between the adsorbed ibuprofen molecules creating a steric barrier. In general, the results showed that temperature is an important parameter to control the efficiency of ibuprofen removal.

3.6 Photocatalytic degradation of ibuprofen

Optimization of adsorption condition only achieved 22% of ibuprofen removal on α-Fe_2O_3. The low surface area and non-porosity of iron oxide may restrict the number of available site for ibuprofen adsorption. Since iron oxide has band gap of energy at 2.3 eV that can utilize photon energy up to 600 nm (Zhou et al., 2010), its activity as photocatalyst was evaluated for degradation of ibuprofen. Figure 11 shows the effect of UV-light irradiation on the removal of ibuprofen using α-Fe_2O_3-G500. Three sets of experiments were conducted; in dark to represent adsorption, immediate light irradiation and light irradiation after 20 min of adsorption. It is apparent that photocatalytic degradation of ibuprofen using α-Fe_2O_3-G500 increased the removal efficiency up to 53%. When compared with treatment without UV light (dark adsorption only), the removal of ibuprofen only reached 28%. However, the combination of adsorption treatment followed by UV irradiation increased the ibuprofen removal up to 80%.

The activity of iron oxide as photocatalyst significantly improved the removal of ibuprofen via photodegradation. Preliminary adsorption prior to irradiation optimized the interaction between ibuprofen and iron oxide. Photodegradation process can take place by direct reaction of hydroxyl radical with the adsorbed ibuprofen on the surface of photocatalysts (Eq. 5-8). This process occurs faster due to efficient charge transfer from Fe_2O_3 surface to the adsorbed substrate. In photocatalytic degradation without prior adsorption, the photogenerated electron and hole formed mobile $OH^{\bullet}$ radical in the solution via superoxide radicals intermediate (Eq. 9-12) (Sanad et al., 2021). The $OH^{\bullet}$ radical diffuse to oxidize ibuprofen to presumably CO_2 and H_2O (Eq. 14). There is a possibility of $OH^{\bullet}$ radical to recombine and released heat.

Preprints (www.preprints.org) | NOT PEER-REVIEWED | Posted: 8 October 2021 doi:10.20944/preprints202110.0138.v1

Adsorption of ibuprofen

$C_3H_{18}O_2 \rightarrow C_3H_{18}O_2(a)$ (Eq. 5)

Electron excitation

$\alpha\text{-}Fe_2O_3 \rightarrow \alpha\text{-}Fe_2O_3 (e^- + h^\bullet)$ (Eq. 6)

Electron trapping by surface hydroxyl group

$e^- + OH(a) \rightarrow OH^\bullet(a)$ (Eq. 7)

Direct decomposition of adsorbed ibuprofen

$C_3H_{18}O_2(a) + OH^\bullet(a) \rightarrow CO_2 + H_2O$ (Eq. 8)

Electron trapping by dissolved oxygen to form superoxide radicals

$e^- + O_2 \rightarrow O_2^{\bullet-}$ (Eq. 9)

Water dissociation

$H_2O \rightarrow H^+ + OH^-$ (Eq. 10)

Generation of hydroxyl radical

$O_2^{\bullet-} + H^+ + H_2O \rightarrow H_2O_2 + O_2$ (Eq. 11)

$H_2O_2 \rightarrow 2OH^\bullet$ (Eq. 12)

Hole trapping

$OH^- + h^+ \rightarrow OH^\bullet$ (Eq. 13)

Ibuprofen degradation

$OH^\bullet + C_3H_{18}O_2 \rightarrow CO_2$ and H_2O (Eq. 14)

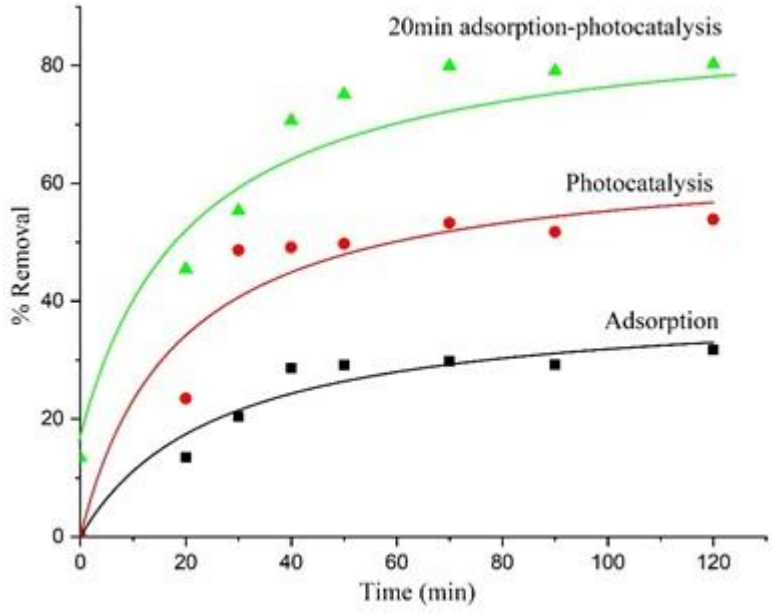

Figure 11. Photocatalytic removal of ibuprofen using Fe_2O_3-G-500. Three sets of experiment were conducted to show the efficiency of hematite in photodegradation of ibuprofen; (i) immediate UV light irradiation for 120 min, (ii) dark adsorption and (iii) 20 min dark adsorption folowed by UV irradiation for 120 min.

4. Conclusions

Iron oxide (Fe_2O_3-G) with uniform hexagonal flake morphology has been successfully synthesized using a combination of gelatin as a natural template and F127 as a synthetic

template via sol-gel method. SEM analysis showed the formation of uniform hexagonal flake-like structure that was stable after calcination at 500 °C. The transition from hexagonal to cubic structure was observed after calcination at 700 °C. Gelatin as naturally formed polymer showed a potential as structure directing agent for the formation of a highly stable iron oxide with uniform structures. The adsorption capacity of Fe_2O_3-G as adsorbent for ibuprofen was determined at 55 mg/g when using the hexagonal flake-like iron oxide. Although the calcination at 700 °C produced a high purity iron oxide, the adsorption capacity and removal efficiency were significantly reduced due to the formation of low surface area cubic crystallites. The efficiency of the adsorption was strongly depended on the surface area of iron oxide. The combination of photocatalytic degradation and adsorption for the removal of ibuprofen using iron oxide resulted in the increase of removal efficiency to 80% under UV light irradiation.

Supplementary Materials: The following are available online at www.mdpi.com/xxx/s1, Figure S1: title, Table S1: title, Video S1: title.

Author Contributions: For research articles with several authors, a short paragraph specifying their individual contributions must be provided. The following statements should be used "Conceptualization, X.X. and Y.Y.; methodology, X.X.; software, X.X.; validation, X.X., Y.Y. and Z.Z.; formal analysis, X.X.; investigation, X.X.; resources, X.X.; data curation, X.X.; writing—original draft preparation, X.X.; writing—review and editing, X.X.; visualization, X.X.; supervision, X.X.; project administration, X.X.; funding acquisition, Y.Y. All authors have read and agreed to the published version of the manuscript." Please turn to the CRediT taxonomy for the term explanation. Authorship must be limited to those who have contributed substantially to the work reported.

Funding: This research was funded by DIKTI, grant number ID 221.1/UN27.22/HK 07.00/2021/on Scheme Fundamental Research (Penelitian Dasar) 2021 under Maria ulfa

Acknowledgments: Author acknowledges the financial support of DIKTI, grant number ID 221.1/UN27.22/HK 07.00/2021 on Scheme Fundamental Research (Penelitian Dasar) 2021 under Maria ulfa

Conflicts of Interest: The authors declare no conflict of interest.

References

Campos, I., Espindola, A., Chagas, C., Barbosa, E., Castro, C. E., Molina, C., Fonseca, F. L. A., & Haddad, P. S. (2020). Biocompatible superparamagnetic nanoparticles with ibuprofen as potential drug carriers. *SN Applied Sciences*, *2*(3). https://doi.org/10.1007/s42452-020-2265-7

Cao, Y. Q., Zi, T. Q., Zhao, X. R., Liu, C., Ren, Q., Fang, J. Bin, Li, W. M., & Li, A. D. (2020). Enhanced visible light photocatalytic activity of Fe2O3 modified TiO2 prepared by atomic layer deposition. *Scientific Reports*, *10*(1), 1–10. https://doi.org/10.1038/s41598-020-70352-z

Coradin, T., Bah, S., & Livage, J. (2004). Gelatine/silicate interactions: From nanoparticles to composite gels. *Colloids and Surfaces B: Biointerfaces*, *35*(1), 53–58. https://doi.org/10.1016/j.colsurfb.2004.02.008

Haruna, K., Obot, I. B., Ankah, N. K., Sorour, A. A., & Saleh, T. A. (2018). Gelatin: A green corrosion inhibitor for carbon steel in oil well acidizing environment. *Journal of Molecular Liquids*, *264*, 515–525. https://doi.org/10.1016/j.molliq.2018.05.058

Sanad, M. M. S., Farahat, M. M., El-Hout, S. I., & El-Sheikh, S. M. (2021). Preparation and characterization of magnetic photocatalyst from the banded iron formation for effective photodegradation of methylene blue under UV and visible illumination. *Journal of Environmental Chemical Engineering*, *9*(2), 105127. https://doi.org/10.1016/j.jece.2021.105127

Sugrañez, R., Balbuena, J., Cruz-Yusta, M., Martín, F., Morales, J., & Sánchez, L. (2015). Efficient behaviour of hematite towards the photocatalytic degradation of NOx gases. *Applied Catalysis B: Environmental*, *165*(X), 529–536.

https://doi.org/10.1016/j.apcatb.2014.10.025

Yatsenko, D. A., & Medvedeva, T. B. (2019). Estimating Crystality Index of Microcrystalline Cellulose Using Diffraction Methods. *Journal of Structural Chemistry*, *60*(9), 1430–1436. https://doi.org/10.1134/S0022476619090075

Yetiz, E., Ay, E., Uysal, U., & Mualla, O. (2011). Ibuprofen release from porous hydroxyapatite tablets. *Ceramics International*, *37*(7), 2117–2125. https://doi.org/10.1016/j.ceramint.2011.02.021

Zhang, C., Yu, Z., Zeng, G., Huang, B., Dong, H., Huang, J., Yang, Z., Wei, J., Hu, L., & Zhang, Q. (2016). Phase transformation of crystalline iron oxides and their adsorption abilities for Pb and Cd. *Chemical Engineering Journal*, *284*, 247–259. https://doi.org/10.1016/j.cej.2015.08.096

Zhou, X., Yang, H., Wang, C., Mao, X., Wang, Y., Yang, Y., & Liu, G. (2010). Visible light induced photocatalytic degradation of rhodamine B on one-Dimensional iron oxide particles. *Journal of Physical Chemistry C*, *114*(40), 17051–17061. https://doi.org/10.1021/jp103816e

Campos, I., Espindola, A., Chagas, C., Barbosa, E., Castro, C. E., Molina, C., Fonseca, F. L. A., & Haddad, P. S. (2020). Biocompatible superparamagnetic nanoparticles with ibuprofen as potential drug carriers. *SN Applied Sciences*, *2*(3). https://doi.org/10.1007/s42452-020-2265-7

Cao, Y. Q., Zi, T. Q., Zhao, X. R., Liu, C., Ren, Q., Fang, J. Bin, Li, W. M., & Li, A. D. (2020). Enhanced visible light photocatalytic activity of Fe2O3 modified TiO2 prepared by atomic layer deposition. *Scientific Reports*, *10*(1), 1–10. https://doi.org/10.1038/s41598-020-70352-z

Coradin, T., Bah, S., & Livage, J. (2004). Gelatine/silicate interactions: From nanoparticles to composite gels. *Colloids and Surfaces B: Biointerfaces*, *35*(1), 53–58. https://doi.org/10.1016/j.colsurfb.2004.02.008

Haruna, K., Obot, I. B., Ankah, N. K., Sorour, A. A., & Saleh, T. A. (2018). Gelatin: A green corrosion inhibitor for carbon steel in oil well acidizing environment. *Journal of Molecular Liquids*, *264*, 515–525. https://doi.org/10.1016/j.molliq.2018.05.058

Sanad, M. M. S., Farahat, M. M., El-Hout, S. I., & El-Sheikh, S. M. (2021). Preparation and characterization of magnetic photocatalyst from the banded iron formation for effective photodegradation of methylene blue under UV and visible illumination. *Journal of Environmental Chemical Engineering*, *9*(2), 105127. https://doi.org/10.1016/j.jece.2021.105127

Sugrañez, R., Balbuena, J., Cruz-Yusta, M., Martín, F., Morales, J., & Sánchez, L. (2015). Efficient behaviour of hematite towards the photocatalytic degradation of NOx gases. *Applied Catalysis B: Environmental*, *165*(X), 529–536. https://doi.org/10.1016/j.apcatb.2014.10.025

Yatsenko, D. A., & Medvedeva, T. B. (2019). Estimating Crystality Index of Microcrystalline Cellulose Using Diffraction Methods. *Journal of Structural Chemistry*, *60*(9), 1430–1436. https://doi.org/10.1134/S0022476619090075

Yetiz, E., Ay, E., Uysal, U., & Mualla, O. (2011). Ibuprofen release from porous hydroxyapatite tablets. *Ceramics International*, *37*(7), 2117–2125. https://doi.org/10.1016/j.ceramint.2011.02.021

Zhang, C., Yu, Z., Zeng, G., Huang, B., Dong, H., Huang, J., Yang, Z., Wei, J., Hu, L., & Zhang, Q. (2016). Phase transformation of crystalline iron oxides and their adsorption abilities for Pb and Cd. *Chemical Engineering Journal*, *284*, 247–259. https://doi.org/10.1016/j.cej.2015.08.096

Zhou, X., Yang, H., Wang, C., Mao, X., Wang, Y., Yang, Y., & Liu, G. (2010). Visible light induced photocatalytic degradation of rhodamine B on one-Dimensional iron oxide particles. *Journal of Physical Chemistry C*, *114*(40), 17051–17061. https://doi.org/10.1021/jp103816e

Campos, I., Espindola, A., Chagas, C., Barbosa, E., Castro, C. E., Molina, C., Fonseca, F. L. A., & Haddad, P. S. (2020). Biocompatible superparamagnetic nanoparticles with ibuprofen as potential drug carriers. *SN Applied Sciences*, *2*(3). https://doi.org/10.1007/s42452-020-2265-7

Cao, Y. Q., Zi, T. Q., Zhao, X. R., Liu, C., Ren, Q., Fang, J. Bin, Li, W. M., & Li, A. D. (2020). Enhanced visible light

photocatalytic activity of Fe2O3 modified TiO2 prepared by atomic layer deposition. *Scientific Reports*, *10*(1), 1–10. https://doi.org/10.1038/s41598-020-70352-z

Coradin, T., Bah, S., & Livage, J. (2004). Gelatine/silicate interactions: From nanoparticles to composite gels. *Colloids and Surfaces B: Biointerfaces*, *35*(1), 53–58. https://doi.org/10.1016/j.colsurfb.2004.02.008

Haruna, K., Obot, I. B., Ankah, N. K., Sorour, A. A., & Saleh, T. A. (2018). Gelatin: A green corrosion inhibitor for carbon steel in oil well acidizing environment. *Journal of Molecular Liquids*, *264*, 515–525. https://doi.org/10.1016/j.molliq.2018.05.058

Sanad, M. M. S., Farahat, M. M., El-Hout, S. I., & El-Sheikh, S. M. (2021). Preparation and characterization of magnetic photocatalyst from the banded iron formation for effective photodegradation of methylene blue under UV and visible illumination. *Journal of Environmental Chemical Engineering*, *9*(2), 105127. https://doi.org/10.1016/j.jece.2021.105127

Sugrañez, R., Balbuena, J., Cruz-Yusta, M., Martín, F., Morales, J., & Sánchez, L. (2015). Efficient behaviour of hematite towards the photocatalytic degradation of NOx gases. *Applied Catalysis B: Environmental*, *165*(X), 529–536. https://doi.org/10.1016/j.apcatb.2014.10.025

Yatsenko, D. A., & Medvedeva, T. B. (2019). Estimating Crystality Index of Microcrystalline Cellulose Using Diffraction Methods. *Journal of Structural Chemistry*, *60*(9), 1430–1436. https://doi.org/10.1134/S0022476619090075

Yetiz, E., Ay, E., Uysal, U., & Mualla, O. (2011). Ibuprofen release from porous hydroxyapatite tablets. *Ceramics International*, *37*(7), 2117–2125. https://doi.org/10.1016/j.ceramint.2011.02.021

Zhang, C., Yu, Z., Zeng, G., Huang, B., Dong, H., Huang, J., Yang, Z., Wei, J., Hu, L., & Zhang, Q. (2016). Phase transformation of crystalline iron oxides and their adsorption abilities for Pb and Cd. *Chemical Engineering Journal*, *284*, 247–259. https://doi.org/10.1016/j.cej.2015.08.096

Zhou, X., Yang, H., Wang, C., Mao, X., Wang, Y., Yang, Y., & Liu, G. (2010). Visible light induced photocatalytic degradation of rhodamine B on one-Dimensional iron oxide particles. *Journal of Physical Chemistry C*, *114*(40), 17051–17061. https://doi.org/10.1021/jp103816e

Yetiz, E., Ay, E., Uysal, U., & Mualla, O. (2011). Ibuprofen release from porous hydroxyapatite tablets. *Ceramics International*, *37*(7), 2117–2125. https://doi.org/10.1016/j.ceramint.2011.02.021

Banerjee, P., Das, P., Zaman, A., & Das, P. (2016). Application of graphene oxide nanoplatelets for adsorption of Ibuprofen from aqueous solutions : Evaluation of process kinetics and. Process Safety and Environmental Protection, 101, 45–53. https://doi.org/10.1016/j.psep.2016.01.021

Das, P., Banerjee, P., Rathour, R., Misra, R., 2014. Assessment on linear and non-linear analysis for the estimation of pseudo-second-order kinetic parameters for removal of dye using graphene nanosheet. Desalin. Water Treat., http://dx.doi.org/10.1080/19443994.2014.937759.

Das, P., Banerjee, P., Mondal, S., 2015. Mathematical modelling and optimization of synthetic textile dye removal using soil composites as highly competent liner material. Environ. Sci. Pollut. Res. 22, 1318–1328.

Satapathy, M.K., Banerjee, P., Das, P., 2013. Plant-mediated synthesis of silver-nanocomposite as novel effective azo dye adsorbent. Appl. Nanosci. 5, 1–9.

G. Pedroza-Herrera, I.E. Medina-Ramírez, J.A. Lozano-Álvarez, S.E. Rodil, Evaluation of the Photocatalytic Activity of Copper Doped TiO2 nanoparticles for the Purification and/or Disinfection of Industrial Effluents, Catalysis Today, (2018).

M.C. Wu, P.Y. Wu, T.H. Lin, T.F. Lin, Photocatalytic performance of Cu-doped TiO2 nanofibers treated by the hydrothermal synthesis and air-thermal treatment, Applied Surface Science 430 (2018) 390–398.

A. Shafei, S. Sheibani, Visible light photocatalytic activity of Cu doped TiO2-CNT nanocomposite powder prepared by sol–gel method, Materials Research Bulletin 110 (2019) 198–206

 doi:10.20944/preprints202110.0138.v1